Journal of New Materials for Electrochemical Systems 16, 257-262 (2013)
© J. New Mat. Electrochem. Systems

Short Communication

A Ferric-Air Battery base on Solid Oxide Fuel Cell for Electrical Energy Storage

Ting Luo, Shaorong Wang*, Le Shao, Jiqing Qian, Xiaofeng Ye, Zhongliang Zhan and Tinglian Wen

CAS Key Laboratory of Materials for Energy Conversion, Shanghai Institute of Ceramics,
Chinese Academy of Sciences (SICCAS), P.R. China

Received: March 06, 2013, Accepted: April 06, 2013, Available online: May 28, 2013

Abstract: *We report a ferric-air, solid oxide battery that consists of a tubular solid oxide cell with $Ca(OH)_2$/CaO dispersed Fe/FeOx powders integrated as the redox-active materials in the fuel chamber. The key feature here is the use of $Ca(OH)_2$ to prevent agglomeration and coarsening of Fe/FeO_x powders, and more importantly to enable in situ production of H_2/H_2O as the electrochemical active redox couple in the fuel electrode. The proof-of-concept solid oxide battery exhibits an energy capacity of 144 Wh kg^{-1}-Fe at a ferric utilization of 18.8% and excellent stability in ten discharge/charge cycles with a voltage efficiency of 83% that have great potential for improvement. These results showed encouraging promise of the ferric-air, solid oxide batteries for electrical energy storage applications.*

Keywords: Ferric-Air battery, solid oxide fuel cell, electrical energy storage, Tubular design

1. INTRODUCTION

The drastically increased interest in the electrical energy storage systems stems from urgent demand for improved power reliability and quality, a mass penetration of intermittent renewable energy sources and the transition of the electricity network to a smart grid. Among various electric energy storage systems, electrochemical energy storage exhibits distinctive features such as high round-trip efficiencies, flexibility in power and energy densities, a long deep-cycle life, pollution-free operation and low maintenance costs, and is thereby set to become critically important in the near future, despite the fact that the existing energy storage is dominated by hydroelectric water pumping and underground compressed air storage that are limited to some specific natural geographic sites [1-4]. For secondary batteries, the electrical energy is stored within the electrode structure via charge transfer reactions that nevertheless results in low specific energy densities and small system capacity. For example, typical practical specific energy of sodium-sulfur batteries is in the range of 150-240Wh kg^{-1}. Lithium ion batteries exhibited a typical practical energy density of 150-200 Wh kg^{-1} [5-8]. In contrast, redox-flow batteries can provide much more scalable electrical energy storage by circulating two soluble and electrochemically active redox couples that are oxidized and reduced to store or release energy. Nonetheless, low solubility of redox couples (< 8 M) usually do not allow their specific energy densities to exceed 25 Wh kg^{-1}, which make the redox-flow battery system bulky, massive and costly [9-10].

Solid oxide fuel cells (SOFCs) offer very high efficiency in the conversion of chemical energy from a variety of fuels to electricity. Large scale power generation has been demonstrated by Siemens Westinghouse and Bloom energy et al. with excellent stability. Traditional SOFCs research has focused on fuel variability, using methane, diesel or coal, instead of hydrogen, for the early commercialization. Recently the concept of reversible solid oxide cells [11-13], where energy can be transformed into hydrogen via electrolysis of steam or water for later conversion back into electricity in the fuel cell mode, have shown great promise for integration with renewable energy sources such as solar and wind. Such a technology is reasonable, because most SOFCs work the best with hydrogen as fuel. However, the concept of fuel cell limited our thoughts to the devices that require large volume of hydrogen storage and pumping lines for gas transfer, and the active materials are stored outside of the cell. Recently, Huang and Xu[14] reported a solid oxide redox flow batter that consisted of a reversible solid oxide cell and a separate Fe/FeO redox-cycle unit in a closed-loop fashion as created by a circulating pump and a set of toggle valves. Such a new storage battery yielded an energy capacity of 348 Wh kg^{-1}-Fe and a round- trip efficiency of 91.5% over twenty stable

*To whom correspondence should be addressed: Email: srwang@mail.sic.ac.cn

charge/discharge cycles with ten minutes for a single-cycle period at a relatively low Fe loading (0.11 g) and utilization (38.5%). Zhao and Huang [15] investigated that the iron utilization played a determining role in storage capacity and round-trip efficiency. In these papers electrical pump is required to achieve a closed-loop circulation of the reaction gas and thereby stabilize power and energy outputs. This makes the system more complexity and may be responsible of the parasitic losses and the decrease in the overall efficiency. The difference between our paper and the ref. [14]-[15] is the use of the need of water circulation in these references. In our paper, steam was produced by the decomposition of $Ca(OH)_2$ at high temperature, instead of using a circulation unit of H_2O / H_2. The merit of this design is the reduction of unnecessary volume for reaction chamber and no requirement of cycling pump, which means simplicity in system design and reduction of operating cost.

Here we report a novel solid fuel for the reversible SOFCs that consisted of a tubular solid oxide cell integrated with $Ca(OH)_2$/CaO dispersed Fe/FeO_x powders as the redox-active material inside of the fuel chamber. Thermo-gravimetric analysis indicated that $Ca(OH)_2$ started to decompose at temperatures above 500°C, *i.e.*,

$$Ca(OH)_2 = CaO + H_2O \quad (1)$$

The resulting steam further reacts with ferric powders to produce hydrogen, which diffuses into the Ni-SSZ electrode and is then electrochemically oxidized to produce electricity. Based upon the predominance area diagram of Fe-Fe oxides (Fig. 1), the ferric oxidation product should be magnetite, Fe_3O_4, at T < 570°C or iron monoxide, FeO, at T > 570°C. Since the tubular solid oxide cell with the redox materials inside the fuel chamber was usually maintained at 800°C, FeO was the dominant oxidation product in the present paper.

$$Fe + H_2O = FeO + H_2 \quad (2)$$

$$H_2 + O^{2-} = H_2O + 2\,e^- \quad (3)$$

Note that steam is replenished via the electrochemical oxidation reaction (3) that would enable reaction (2) and (3) to proceed simultaneously and continuously during the discharge mode until all the ferric powders are consumed or a desired ferric utilization is achieved. Once the discharging mode is turned off, both reactions can be immediately stopped. By combining reaction (2) and (3), the overall anodic reaction in the discharging mode can be expressed as:

$$Fe + O^{2-} = FeO + 2e^- \quad (4)$$

During the charging mode, electrolysis of steam occurs in the Ni-SSZ electrode, and the resultant hydrogen diffuses into the fuel chamber and reduces FeO to Fe.

$$H_2O + 2e^- = H_2 + O^{2-} \quad (5)$$

$$FeO + H_2 = Fe + H_2O \quad (6)$$

Different from the discharging mode, steam is replenished via chemical reaction (6), such that reaction (5) and (6) can proceed progressively and electricity is continuously stored. By combining reaction (5) and (6), the overall cathodic reaction in the discharging mode is

$$FeO + 2e^- = Fe + O^{2-} \quad (7)$$

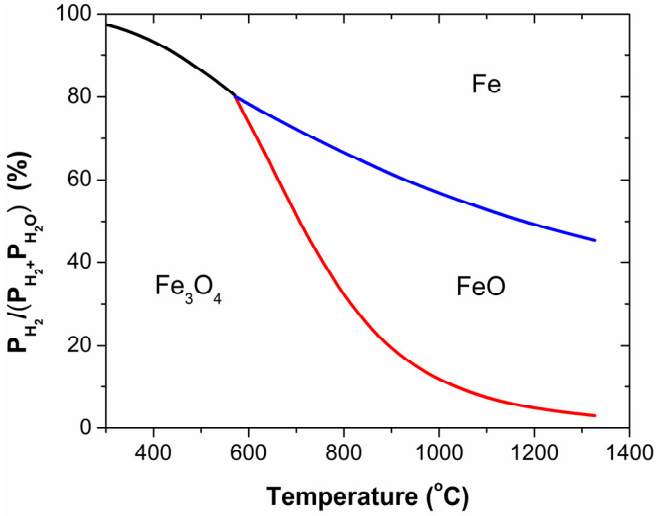

Figure 1. The predominance area diagram of Fe-Fe oxides.

In the air electrode, oxygen reduction reaction (ORR) and oxygen evolution reaction (OER) occurs during the discharging and charging mode, respectively.

$$1/2\ O_2 + 2e^- = O^{2-} \quad (8)$$

From reactions (4), (7) and (8), the overall reaction for the present ferric-air battery can be simply written as

$$Fe + 1/2\ O_2 = FeO \quad (9)$$

Notably, the solid oxide cell integrated with $Ca(OH)_2$/CaO dispersed ferric powders in the fuel chamber behaviours like a ferric-air battery. Therefore, by using Fe powder as original fuel, and $Ca(OH)_2$ / CaO as the auxiliary materials, the H_2/H_2O redox storing cycling can well combine with Fe/FeO redox storing cycling. Then the cell can be sealed as a stand-alone system without any auxiliary equipment for gas transfer. Such a system has a potential merit, the advantages of SOFC, such as high efficiency and excellent power density, can find their way in the application of EES in a compact and low cost mode.

2. EXPERIMENTAL

2.1. The preparation of the cell and redox material

The solid oxide cell used in the present study consisted of a tubular Ni-SSZ fuel electrode support, a thin SSZ electrolyte and a thin LSM-SSZ oxygen electrode (SSZ = 6 mol% Sc_2O_3 stabilized ZrO_2, LSM = $La_{0.8}Sr_{0.2}MnO_3$) were fabricated using slip casting, dip-coating, and co-sintering techniques as previously reported [16]. The tube was 20 cm long with an inner and outer diameter of 8 and 10 mm, respectively. The length of the air electrode coating was typically 0.3-2 cm that gave an effective working area of 0.94-6.28cm^2. The redox material was prepared by ball milling powders of ferric and $Ca(OH)_2$ powders in a mole ratio of 0.35:1, then all the powders were installed into the fuel chamber of the solid oxide cell.

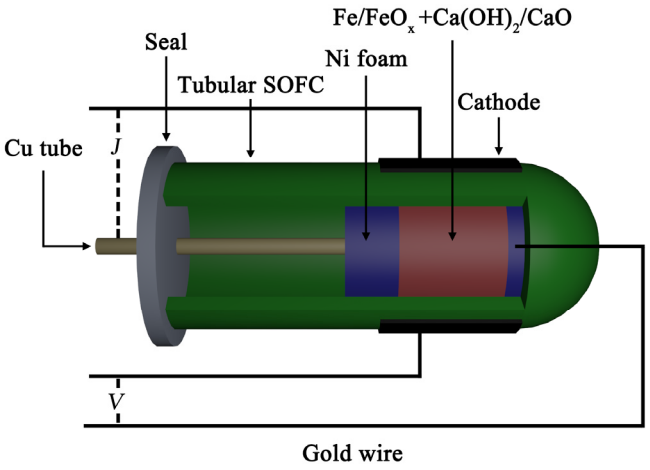

Figure 2. Schematic illustration of the ferric-air, solid oxide battery, consisting of a tubular solid oxide cell integrated with $Ca(OH)_2$ dispersed Fe as the redox-active materials in the fuel chamber.

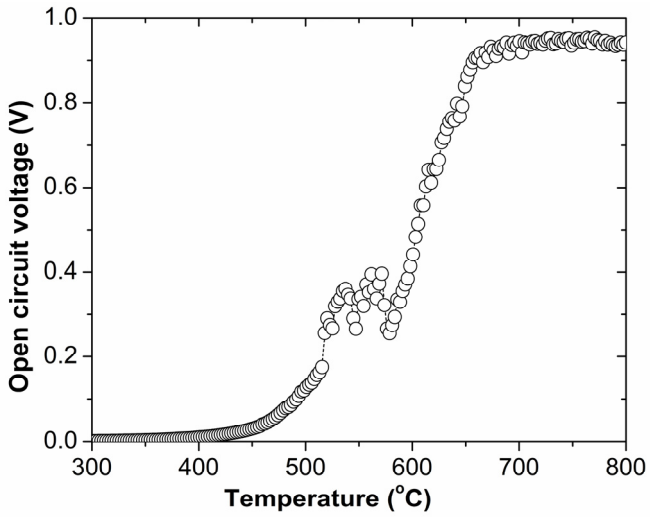

Figure 3. Temperature dependence of the open circuit voltage for the cell when the temperature up to 800°C.

2.2. Assembling battery and test

A schematic design of the tubular cell testing setup is represented in Fig. 2. The tubular SOFC anode firstly was reduced by H_2 at 750℃, and cooled down to ambient temperature using H_2 as the protective atmosphere all the time. The Cu tube was wrapped by Ni foam tightly and then inserted into the fuel chamber, which was used to collect the current from the fuel electrode. In addition, the Cu tube was also designed for gas ventilation. A small hole was drilled at the closed-end side of the cell, where a gold wire was attached to the fuel electrode and served as the voltage lead. The hole was then sealed using a glass ink. Fe and $Ca(OH)_2$ powders were ball-milled and then loaded into the fuel chamber. 10% Hydrogen balanced by nitrogen was introduced into the fuel chamber to purge out air through the Cu tube. Finally, the cell was vacuumed to 0.001Mpa and sealed using stainless steel lid and silica gel. During the discharging process, Fe reacts with H_2O generated from the decomposition of $Ca(OH)_2$ at high temperature, as a result, H_2 is produced in situ as SOFC fuel. After reaction with O^{2-}, H_2O is produced and it continually reacts with the rest Fe, as shown in Eq. (1)-(3). Once stopping discharging, the reactions can be ceased immediately. The charging process is realized by electrolysis of water in the SOEC mode along with the reduction of FeO by the generated H_2, as shown in Eq.(6).

For evaluating the electrochemical characteristics of the Fe-air battery, oxygen was maintained on the air electrode at a flow rate of 30 mL min^{-1}. The operation temperature was set at 800°C. Current-voltage (I-V) curves and the electrochemical impedance spectra (EIS) were obtained by using an Electrochemical Workstation IM6ex (Zahner, GmbH, Germany). The EIS were recorded with a perturbation voltage of 20mV over the frequency range 0.1Hz to 100 kHz.

3. RESULTS AND DISCUSSION

Fig. 3 shows the temperature dependence of the open circuit voltage (OCV) of the present Fe-air battery when the temperature was heated up to 800°C. The OCV increased with increasing temperature, and tended to be stabilized around 0.94-0.95 V at 800°C. Note that FeO is only stable at T>570°C, and would disproportionate at T<570°C to produce metallic ferric and magnetite, Fe_3O_4 (Fig. 1). The abrupt change in the temperature range of 520°C-580°C is attributed to the production of H_2O from $Ca(OH)_2$.

Fig. 4 (a) shows the typical voltage V versus current density J dependence for the present Fe-air battery in the discharging and charging modes at 800°C. As previously observed for steam electrolysis in solid oxide electrolysis cells, the slope of the J-V curve does not change for the cell transitioning from one mode to the other [17]. The linear J-V dependence was further confirmed by almost the same electrochemical impedance spectra (Fig. 4 b and c) obtained at a discharging or charging current density of 70 mA cm^{-2}, demonstrating good reversibility of the battery electrodes for charge transfer reactions. The discharging current density at V = 0.7 V was 138 mA cm^{-2} and the charging current density at 1.3 V was about 286 mA cm^{-2}, which were very comparable to the performance of solid oxide cells achieved when respectively operating on 97% H_2 – 3% H_2O and 25% H_2 -75% H_2O gases continuously replenished at 100 sccm (Fig. 4 b and c). Such a discharging current density for the present cell is substantially larger than ~ 5 mA cm^{-2} for lithium ion batteries, 0.01~10 mA cm^{-2} for Li-air batteries, or 20-100mA cm^{-2} for the all vanadium redox flow batteries [1, 18]. The superior rating capability can be ascribed to independent roles of the solid oxide cells for electrochemical reactions, and of the Fe/FeO redox unit for energy production and storage.

Note that mass diffusion limitation was not observed in Fig. 4 (a) that would result in abrupt voltage decrease or increase at high current densities in the discharging or charging mode, even though the battery stayed nominally stagnant without any external circulation to create dynamic flow in the fuel chamber. This suggests that reaction (2) proceeds at a rate that is comparable to or even higher than the rate of electrochemical hydrogen oxidation in this discharging mode, whereas the rate of reactions (6) is fast enough to

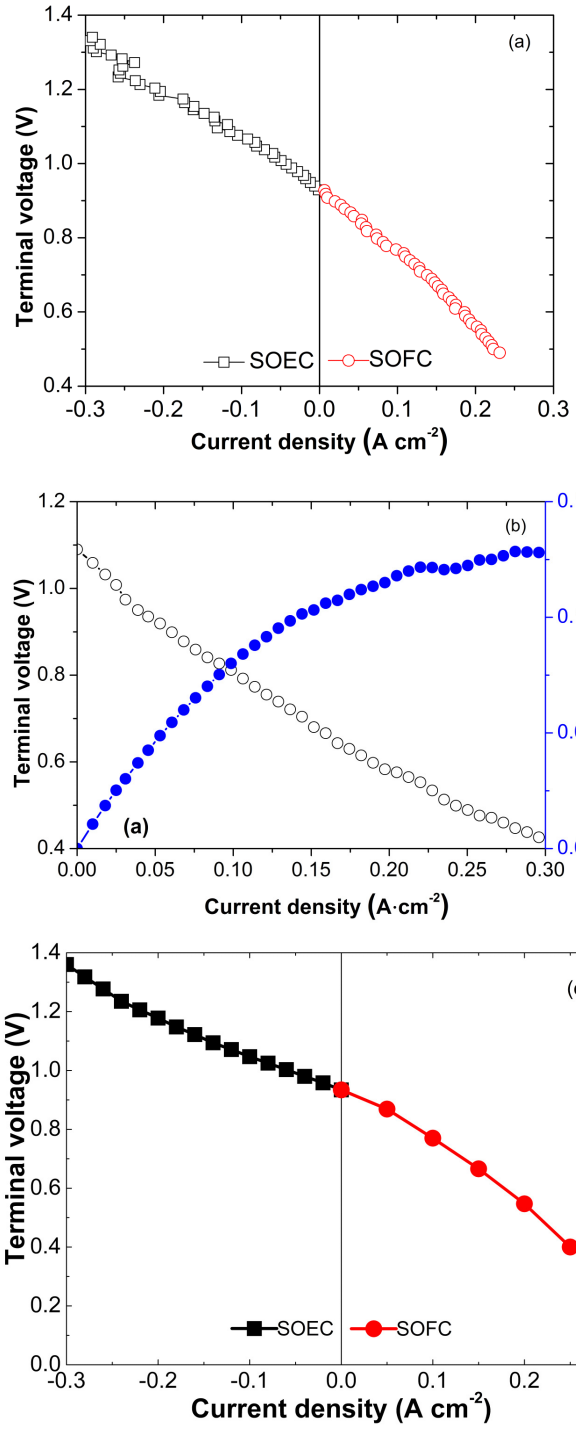

Figure 4. Typical voltage V versus current density J for the present Fe-air battery in both discharging and charging modes at 800°C (a); typical *V* versus *J* for the traditional tubular solid oxide cells at 800°C operating on (b) 97% H_2 - 3% H_2O fuels at 100 sccm in the fuel cell mode, or (c) 25% H_2 – 75% H_2O at 100 sccm in both the fuel cell and the electrolysis modes.

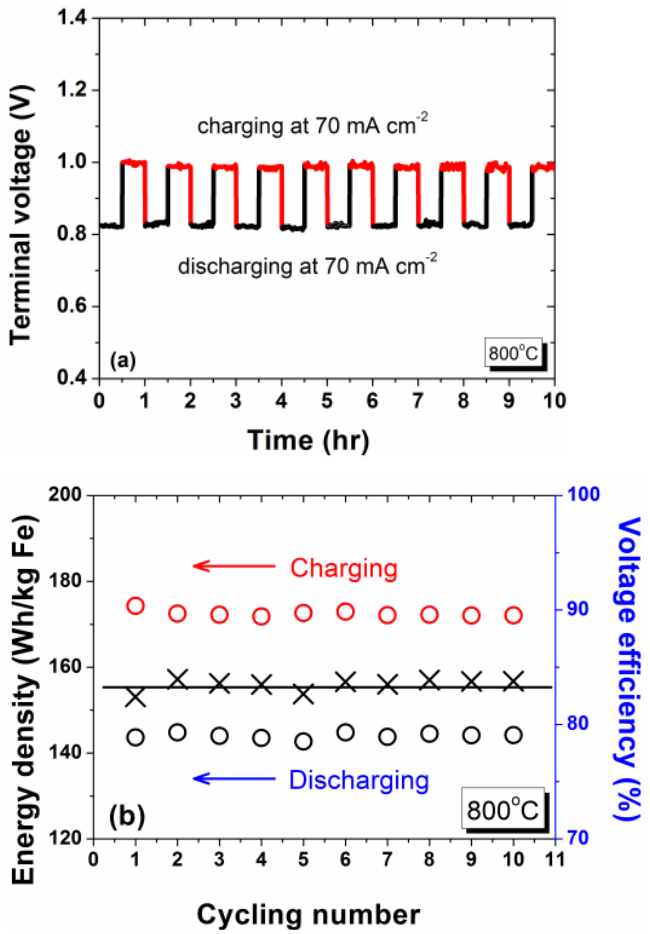

Figure 5. Characters of the present Fe-air battery at 800°C: (a) discharging and charging characteristic and (b) charging efficiency at J = 70 mA cm^{-2}. Ten cycles of repeated discharging and charging were performed, and the duration for discharging and charging in each cycle was 30 minutes.

keep pace with the rate at which steam is electrolyzed at the Ni-SSZ electrode during the charging mode. Furthermore, hydrogen and steam diffused between the Ni-SSZ electrode and the Fe/FeO redox unit at rates no less than for reaction (2-3) in the discharging mode or for reaction (5-6) in the diffusion law and using gas diffusion coefficients (5.74 cm^2 s^{-1} for H_2 and 3.80 cm^2 s^{-1} for H_2O at 800°C), the equilibrium H_2 and H_2O partial pressure in the redox unit as well as the diffusion gap between the redox unit and the Ni-SSZ electrode, a simple calculation indicated that the maximum current density obtainable can be as high as 10 A cm^{-2} in the discharging mode and 6 A cm^{-2} in the charging mode, which are high enough to avoid mass diffusion limitation in the present cell.

Good cycling behavior and high reversible specific energy capacity are critically important for the electrochemical energy storage systems. In order to evaluate the cycling stability of the present ferric-air battery, repeated discharging and charging were performed at a fixed current density of 70 mA cm^{-2} with durations of 30 minutes for discharging and charging in each cycle. Fig. 5 (a) shows the typical discharging and charging characteristic of the cell

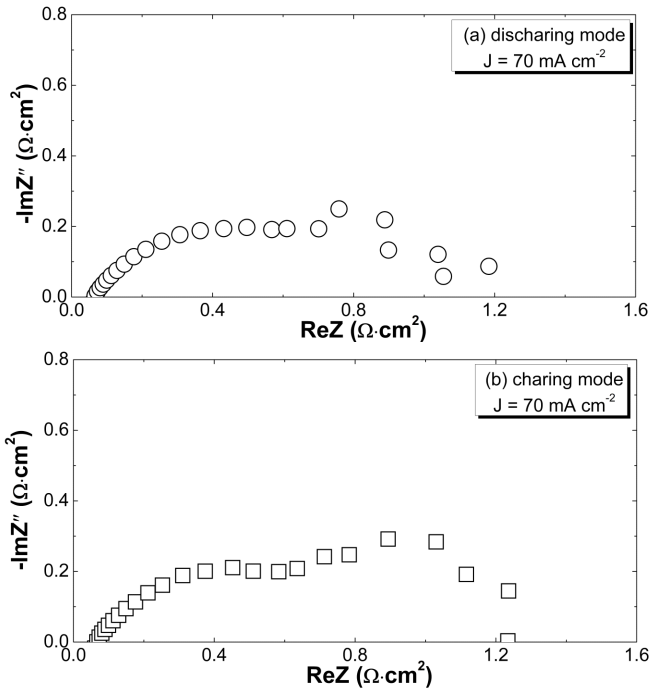

Figure 6. Nyquist plots of electrochemical impedance for the present Fe-air battery at a current density of 70 mA cm^{-2} in the (a) discharging and (b) charging mode.

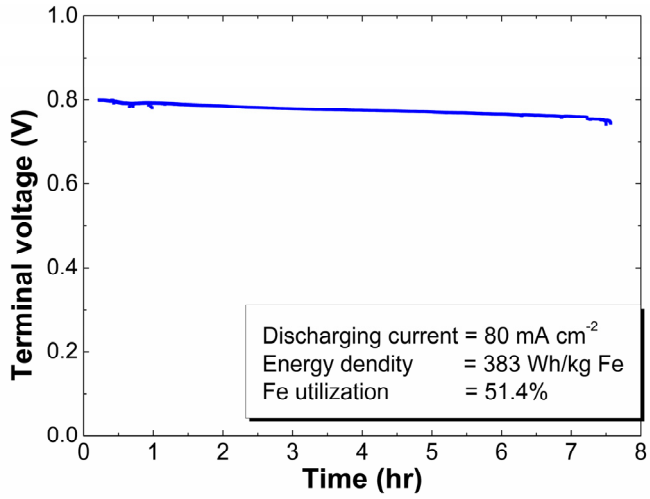

Figure 7. Discharging characteristics of a Fe-air battery loaded with 1.22 g Fe powders. The working area was 1 cm^2.

in ten consecutive cycles. The cell exhibited immediate response for the transitions between the discharging and charging mode, and the terminal voltage stayed almost constant only with slight fluctuations during the discharging or charging process with rapid provision of hydrogen from the chemical reaction (2), or of steam from the chemical reaction (6) before the full consumption of Fe/FeO.

Fig. 5 (b) shows the superior cycling stability and high reversible energy capacities for the present cell, which can be explained by the reversible and kinetically fast reaction of ferric and steam to produce hydrogen and ferric monoxide, the benefit of low density CaO in the Fe/FeO redox unit to prevent ferric agglomeration, and more importantly the well-maintained structural integrity and catalytic activity for electrochemical reactions in the Ni-SSZ electrode that has been free from the large volume expansion-contraction in the neighbouring Fe/FeO redox unit during the discharge-charge cycling process. The average energy densities during each discharging and charging cycle were respectively 144 and 172 Wh kg^{-1} Fe, yielding a voltage efficiency of 83%. Note that the voltage efficiency for the Fe-air battery can be further improved by reducing the discharging/charging current densities as suggested from the $J \sim V$ curves shown in Fig. 4 (a). Alternatively, reducing the internal resistance and improving the electrochemical performance of the solid oxide cell can decrease the slope of the $J \sim V$ curves in Fig. 4 (a) and thereby also increases the voltage efficiency. The internal resistance for the present tubular cell was as high as 1.2 W cm^2 (Fig. 6), which is much larger than the typical 0.3 W cm^2 for the state-of-the-art planar cells and therefore has some great potential for improvement [19].

The overall energy capacity for the present Fe-air battery is largely determined by the ferric loading in the fuel chamber as well as the ferric utilization. For example, a Fe-air battery loaded with 1.22 g Fe powders could provide a stable output of 0.8 V and 80 mA during a discharging duration of 7.5 h, yielding an energy capacity of 383 Wh kg^{-1} Fe at a 51.4% Fe utilization (Fig. 7). Assuming that eighty percent of the fuel chamber (10.05 cm^3) is loaded with $Ca(OH)_2$/CaO dispersed Fe/FeO redox materials (m_{Fe} = 18.3 g), the energy capacity can be as high as 7.2 Wh for the Fe-air battery in the present dimensions at a 51.4% Fe/FeO utilization, yielding an impressive volumetric energy density of 716 WhL^{-1} that is substantially larger than that of 150-250 WhL^{-1} for sodium-sulphur batteries, or 16-33Wh L^{-1} for the all-vanadium redox flow batteries[1].

4. CONCLUSION

In summary, we have demonstrated the viability of a ferric-air battery that integrated a $Ca(OH)_2$ dispersed Fe/FeO redox unit and a tubular solid oxide cell. The unique feature here is in situ production of H_2O from decomposition of $Ca(OH)_2$, and of H_2 from the reversible reaction of ferric and steam. The resulting H_2/H_2O redox is involved in the Ni-SSZ electrode reaction, acting as the catalyst for oxidation of ferric to ferric monoxide. The superior cycling stability can be ascribed to separation of the electrochemical component from the Fe/FeO redox unit that would experience large volume change during the discharge-charge cycling, and the high rating capability was enabled by the rapid, reversible, and comparable kinetics for the chemical Fe/FeO redox reaction and the electrochemical H_2/H_2O redox reaction, as well as the neighbouring positioning that allows for quick transport of H_2/H_2O between the two integrated components and thereby prevents mass diffusion limitation. In contrast to the common solid oxide cells with the redox materials stored outside the cells that increase the system size and complicate the heat management, the present cell can work standalone and safe.

5. ACKNOWLEDGE

The authors gratefully acknowledge the financial support of the National Basic Research Program of China under contract No. 2012CB215400, the National Science Foundation of China under contract No. 51072219, Science and Technology Commission of Shanghai Municipality under contract No. 09JC1415200, 11PJ1410300, 09DZ1206600, Chinese Government High Tech Developing Project under contract No. 2011AA050702, Science and Technology commission of Jiangsu Province under contract No. BK2011006, and the 100 Talents Program of Chinese Academy of Sciences.

REFERENCE

[1] H. Chen, T. N. Cong, W. Yang, C Tan, Y. Li, Y. Ding, Progress in Natural Science, 19, 291 (2009).
[2] B. Dunn, H. Kamath, J.M. Tarascon, Science, 334, 928 (2011).
[3] M. Roeb, H. M€uller-Steinhagen, Science, 329, 773 (2010).
[4] A.S. ARICÒ, P. Bruce, B. Scrosatl, J. Tarascon, W.V. Schalkwijk, nature materials, 4, 366 (2005).
[5] J. Kondoh, I. Ishii, H. Yamaguchi, A. Murata, K. Otani, K. Sakuta, N. Higuchi, S. Sekine, M. Kamimoto, Energy Conversion & anagement, 1, 1863 (2000).
[6] G. Jeong, Y. Kim, H. Kim, Y. Kimd, H. Sohn. Energy Environ. Sci., 4, 1986 (2011).
[7] R. Berthelot, D. Carlier, C. Delmas, Nat. Mater., 10, 74 (2011).
[8] P. Moreau, D. Guyomard, J. Gaubicher, F. Boucher, Chem. Mater., 22, 4126 (2010).
[9] M. Skyllas-Kazacos, M. Rychcik, R.G.Robins, A.G.Fane, M.A. Green, J. Electrochem. Soc., 133, 1057 (1982).
[10]M. Skyllas-Kazacos, G. Kazacos, G. Poon, H. Verseema, Int. J. Energy Res., 34, 182 (2010).
[11]A. Hauch, S.D. Ebbesen, S.H. Jensen, M. Mogensen, J. Mater. Chem., 18, 2331 (2008).
[12]M. Ni, M.K. Leung, D.Y. Leung, Int. J. Hydrogen Enegy, 33, 2337 (2008).
[13]B.C.H. Steele, A. Heinzel, Nature, 414, 345 (2001).
[14]N. Xu, X. Li, X. Zhao, J.B. Goodenough, K. Huang, Energy Environ. Sci., 4, 4942 (2011).
[15]X. Zhao, N. Xu, X. Li, Y. Gong, K. Huang, RSC Advances, 2, 10163 (2012).
[16]R.Z. Liu, S.R. Wang, Bo Huang, C.H. Zhao, J.L. Li, Z.R. Wang, Z.Y. Wen, T.L. Wen., J. Solid State Electrochem., 13, 1905 (2009).
[17]Z. Zhan, W. Kobsiriphat, J.R. Wilson, M. Pillai, I. Kim, S.A. Barnett, Energy & Fuels, 23, 3089 (2009).
[18]M. Rosa Palacion , Chem. Soc. Rev., 38, 2565 (2009).
[19]Z. Zhan, D. Han, T. Wu, X. Ye, S. Wang, T. Wen, S. Cho, S. A. Barnett, RSC Advances, 2, 4075 (2012).